

# Variation Free Molecular Density Functional Theory: Data-driven Stochastic Optimization

Yuriy Kanygin,<sup>\*</sup> Irina Nesterova,<sup>†</sup> Pavel Lomovitskiy,<sup>‡</sup> and Aleksey Khlyupin<sup>§</sup>

*Moscow Institute of Physics and Technology,  
Center for Engineering and Technology of MIPT*

(Dated: December 17, 2020)

Density functional theory (DFT) is an efficient instrument for describing a wide range of nanoscale phenomena: wetting transition, capillary condensation, adsorption, etc. In this paper, we suggest a method for obtaining the equilibrium molecular fluid density in a nanopore using DFT without calculating the free energy variation — Variation Free Density Functional Theory (VF-DFT). This technique can be used to explore confined fluids with a complex type of interactions, additional constraints and to speed up calculations. The fluid density in VF-DFT approach is represented as a decomposition over a limited set of basis functions. We applied principal component analysis (PCA) to extract the main patterns of the confined fluid density and build desired basis functions. The decomposition coefficients of the fluid density by the basis were sought by stochastic optimization algorithms: genetic algorithm (GA), particle swarm optimization (PSO) to minimize the free energy of the system. In this work, two different fluids were studied: nitrogen at a temperature of 77.4 K and argon 87.3 K, at a pore of 3.6 nm, and the performance of optimization algorithms was compared. We also introduce the Hybrid Density Functional Theory (H-DFT) approach based on stochastic optimization methods and the classical Picard iteration method to find the equilibrium fluid density starting from the physically appropriate solution. The combination of these methods helps to significantly speed up the calculations of equilibrium density in the system without losing the quality of the solution, especially in cases with the high pressure and expressed layering structure.

## CONTENT

I. Introduction	1
II. Density Functional Theory	3
III. Variation free method	4
A. Basic patterns analysis	5
B. Stochastic optimization	6
1. Genetic Algorithm (GA)	6
2. Particle Swarm Optimization (PSO)	7
C. Hybrid Density Functional Theory (H-DFT)	7
IV. Results	8
A. Basis functions and problem statement for identical fluids	8
B. Basis functions and problem statement for different fluids	11
V. Conclusion	11
Acknowledgments	11
A. Details for Density Functional Theory	11
References	12

## I. INTRODUCTION

Study of fluids at scales from micro- to nanometers is becoming increasingly crucial for the oil and gas industry (especially for shale hydrocarbons) and the other technology industries [1–7]. There is a large number of tasks in which it is necessary to carry out liquid separation, capture and storage of carbon dioxide, study the flow of liquid in natural or artificial nanoscale structures [1–3, 8]. In particular, for the petroleum industry in unconventional reservoirs, most of the pore space represent structures with a width of several nanometers. On such a scale, classical approaches have limitations, and it becomes necessary to take into account intermolecular forces more accurately to describe such physical phenomena as adsorption [4, 9], electrical double layer formation [1, 5], capillary condensation [1], wetting transition [1, 10], heterogeneity of the reservoir walls [11–14]. An accurate description of these phenomena and the physical properties of materials are extremely important for industry.

One of the most common tools for describing fluids and their interactions with surfaces on such a scale is a molecular density functional theory (DFT) [4, 9, 11, 12, 15–18]. DFT provides a compromise between classical semi-empirical methods and molecular modeling. On the one hand, DFT is capable of taking into account the microscopic structure of a macroscopic system at relatively low computational costs. On the other hand, DFT is a more rigorous theory than classical phenomenological approaches.

According to the mathematical theorem on which the DFT is based, the variation of the free energy with re-

<sup>\*</sup> yuriy.kanygin@phystech.edu

<sup>†</sup> irina.nesterova@phystech.edu

<sup>‡</sup> pavel.lomovitskiy@phystech.edu

<sup>§</sup> khlyupin@phystech.edu

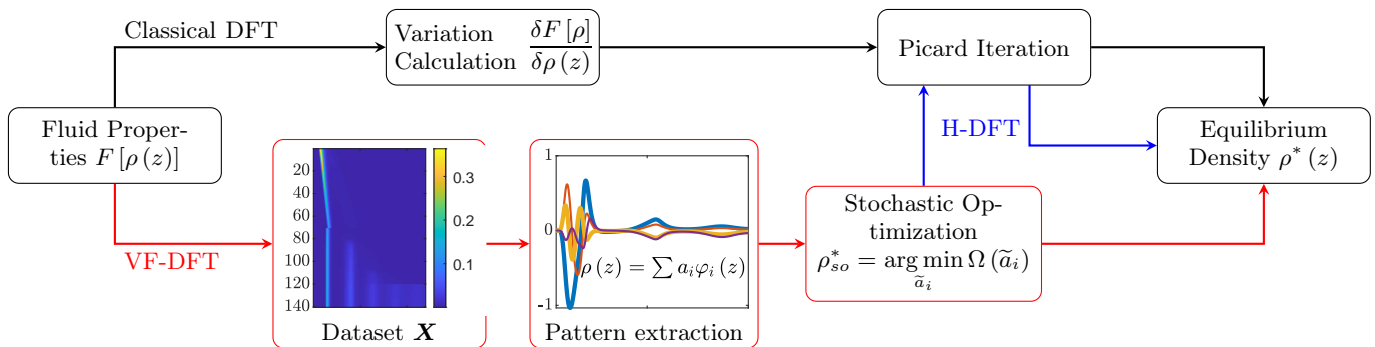


Figure 1: Workflow for the classical DFT with the Picard iterations (black line), the Variation Free DFT method (red line), and the hybrid DFT (red and blue lines)

spect to density must be zero as a necessary condition for the minimum [1, 19], and thus further calculations of the equilibrium density are based on this statement.

The Helmholtz free energy defines the physics of the system, and it has a complex structure for the real fluid. So the variation calculating might be a difficult issue for such systems. Therefore, it is necessary to construct various approximations that describe certain physical phenomena with precise accuracy. Recently developed approaches allowed taking into account the heterogeneity of the surface [11–13], the fluid-fluid interactions [1], or combine DFT with elasticity theories for studying graphene nanobubbles [20]. There are certain subtleties in the last application, fluid in such a system is under additional constrain, and it is crucial to know both the value of system energy and equilibrium density at the same time. The work [11] demonstrated that the physical model complexity and heterogeneity account of the potential interaction of fluid molecules with the surface might significantly change the form of the free energy and its variation. The most significant change undergone the part with the variation of attraction interaction. Depending on what material is being investigated, the variation of free energy has to be calculated in different coordinate systems [21, 22], which means variations should be recalculated in appropriate coordinates. Moreover, for describing polymers or other complex fluids Statistical Associating Fluid Theory (SAFT) is usually used, which considers dispersion, association, and chain contributions in Helmholtz energy [22]. SAFT is an advanced technique for describing real fluids, but it has many modifications for which variations should be calculated.

In this paper, we propose a new approach for calculating the equilibrium density without using Helmholtz free energy variation. The principle operation of VF-DFT algorithm is shown schematically in Fig. 1 compared with the classical DFT, for which it is required to calculate the free energy variations (we have used Picard iterations method). At the initial stage, once for all subsequent tasks, a set of functions is considered, the behavior of which is as close as possible to the studied fluid density. Since the confined fluid structures exhibit typical behav-

ior patterns, these patterns can be efficiently extracted from the set of fluids densities. Especially, in this work, was taken a dataset of equilibrium nitrogen densities at various relative pore pressures of 3.6 nm (these functions were calculated using the classical approach with the Picard iteration method). Also, fluid densities have been added with interaction parameters similar to nitrogen, but with different molecular radii. Adding these "artificial functions" allowed to add a variety to the dataset and apply the algorithm to other fluids. As a result, we got a dataset of 140 different functions.

At the next stage, the most significant patterns are extracted from the dataset using principal component analysis (PCA). The unknown density is represented as an expansion into the calculated basis functions that contain information about the most significant patterns. Thus, finding an equilibrium density is reduced to the problem of optimizing the expansion coefficients. Through the use of PCA, it is possible to reduce the optimization problem's dimension without significant loss of solution quality. Based on the energy criterion, it was possible to decrease the number of optimized decomposition coefficients from 140 to 10. The resulting 10 vectors contain 95 % information [23] about the initial basis.

In the Variation Free algorithm, the search for the density expansion coefficients is carried out using stochastic optimization methods, in contrast to the classical variational approaches, which calculate density based on the Picard iteration or Newton's method [21, 24–27]. Among the wide range of stochastic optimization algorithms, we compared two the most common and popular: genetic algorithm (GA), particle swarm optimization (PSO). Stochastic optimization algorithms have the advantage that they are less affected by local minima and are well applicable for finding global ones. In particular, the algorithm produces a set of expansion coefficients for the density, which corresponds to the equilibrium state of the system and the minimum free energy.

The hybrid algorithm H-DFT combines the advantages of both VF-DFT and classical DFT with Picard iterations. The difference between VF-DFT and H-DFT is the one additional step. After the full calculation of the VF-

DFT solution, it is supplied as an initial approximation for the Picard iteration method. It works faster than classic DFT with the same quality of solutions. However, H-DFT requires free energy variation calculations. Combining these methods reduces the time needed to find the equilibrium density without losing the quality of solutions because the rate of convergence of Picard iterations depends on the choice of the initial approximation. The closer it is to the solution, the faster the method converges.

The developed approach was applied to find the equilibrium fluid density in a pore of 3.6 nm. We considered: nitrogen and argon as fluids, carbon pore walls and planar geometry. The Still potential 10-4-3 [28] was taken as the solid-fluid interaction potential. To describe the fluid-fluid interaction FMT approach was used for hard-sphere repulsion, developed by Rosenfeld [21, 29] and WCA [30] circuit for the attraction interaction. The choice of such fluids and the surface is due to the simplicity of the modelling, and a large amount of data for validation.

As will be shown in section IV, pleasing results are obtained for nitrogen using DFT in a significantly shorter time. In the best case, it turned out that the VF-DFT produced a solution 36 times faster than the classical DFT with Picard iterations. Even though the basis was built based on the fluid with nitrogen parameters, it is possible to calculate the equilibrium density of the fluid, information on which was not in the basis. VF-DFT coped well with the task of calculating the equilibrium density of argon. The advantage of VF-DFT is that it does not need to calculate the variation of the free energy, and the speed of finding a solution is much lower than that of the DFT with Picard iterations. However, the solution quality turns out to be slightly worse than that of the classical DFT and depends on the choice of basic functions. A hybrid H-DFT algorithm based on stochastic optimization methods and the Picard iteration is considered, to maintain the advantage in speed and improve the quality of the obtained solution. The combination of approaches made it possible to speed up calculations of the equilibrium density several times without loss of quality.

The article is organized as follow, in the next section we will provide a brief reference on the density functional theory and the Picard iteration method. Section III will describe a method for basic patterns extraction from data on the density behavior confined system, optimization methods used in this work, and consider the advantages of VF-DFT and H-DFT approaches. Then, in section IV, the results will be considered for nitrogen and argon equilibrium density obtained with the VF-DFT, H-DFT, and classical approach DFT with iterations Picard.

## II. DENSITY FUNCTIONAL THEORY

The density functional theory is based on the fact that the free energy of the system is minimal in equilibrium. For example, for the grand canonical ensemble the free energy is the  $\Omega$ -potential [1, 11, 21]

$$\Omega[\rho(\mathbf{r})] = F[\rho(\mathbf{r})] + \int d^3r \rho(\mathbf{r}) (V_{ext}(\mathbf{r}) - \mu), \quad (1)$$

where  $F[\rho(\mathbf{r})]$  is the Helmholtz free energy,  $\rho(\mathbf{r})$  is a fluid density at the point  $\mathbf{r}$ ,  $V_{ext}$  is the external potential (wall's potential),  $\mu$  is the chemical potential of fluid; temperature, volume and chemical potential are fixed.

The equilibrium density distribution  $\rho(\mathbf{r})$  is meets the following condition [1]

$$\frac{\delta\Omega[\rho(\mathbf{r})]}{\delta\rho(\mathbf{r})} = \frac{\delta F[\rho(\mathbf{r})]}{\delta\rho(\mathbf{r})} + V_{ext}(\mathbf{r}) - \mu = 0. \quad (2)$$

In order to solve Eq. (2), it is necessary to know the form of the Helmholtz energy and its variation. In this paper, we consider fluids nitrogen and argon; therefore, the Helmholtz energy can be divided into the sum of three terms [1]

$$F[\rho] = F^{id}[\rho] + F^{HS}[\rho] + F^{att}[\rho] \quad (3)$$

$$F^{id}[\rho] = k_B T \int d\mathbf{r} \rho(\mathbf{r}) (\ln(\Lambda^3 \rho(\mathbf{r})) - 1) \quad (4)$$

$$F^{HS}[\rho] = k_B T \int d\mathbf{r} \Phi^{RF}[n_\alpha(\rho(\mathbf{r}))] \quad (5)$$

$$F^{att}[\rho] = k_B T \iint d\mathbf{r} \rho(\mathbf{r}) d\mathbf{r}' \rho(\mathbf{r}') U_{att}(|\mathbf{r} - \mathbf{r}'|). \quad (6)$$

The expression Eq. (4) is the ideal part of free energy, where  $k_B$  is the Boltzman's constant,  $T$  is the temperature,  $\Lambda = h/\sqrt{2\pi m T}$  is the thermal de Broglie wavelength,  $h$  - Planck's constant, and  $m$  is the gas molecule mass.

The Eq. (5) takes into account the hard sphere repulsion between fluid particles. The integrand is the Rosenfeld functional  $\Phi^{RF}[n_\alpha(\rho(\mathbf{r}))]$  with weighted density  $n_\alpha(\rho(\mathbf{r}))$  [21, 29]. Currently, there are several modifications to this functional. In this work, we use the classic form obtained by Rosenfeld according to Fundamental Measure Theory (FMT):

$$\Phi^{RF} = -n_0 \ln(1 - n_3) + \frac{n_1 n_2 - \mathbf{n}_1 \cdot \mathbf{n}_2}{1 - n_3} + \frac{n_2^3 - 3n_2 \mathbf{n}_2 \cdot \mathbf{n}_2}{24\pi(1 - n_3)^2}, \quad (7)$$

functions  $n_\alpha, \mathbf{n}_\beta$  is the weighted densities ( $\alpha = 1, 2, 3; \beta = 1, 2$ ), expressions for them can be found in the appendix A.

The Eq. (6) takes into account the contribution of the dipole-dipole interaction to the Helmholtz energy. Attraction potential  $U_{att}$  is the Lennard-Jones potential, which is modified according to the WCA scheme [1, 30].

$$U_{att}(r) = \begin{cases} -\varepsilon_{ff} & r < \lambda \\ U_{LJ} & \lambda < r < r_{cut} \\ 0 & r > r_{cut} \end{cases} \quad (8)$$

where  $\lambda = 2^{1/6}\sigma_{ff}$  is the coordinate of the Lennard-Jones potential minimum,  $\sigma_{ff}$  is the fluid particle diameter  $\varepsilon_{ff}$  is the Lennard-Jones potential value at the minimum and

$r_{cut}$  — cut-off distance (in our work  $r_{cut} = 5\sigma_{ff}$ ),

$$U_{LJ} = 4\varepsilon_{ff} \left( \left( \frac{\sigma_{ff}}{r} \right)^{12} - \left( \frac{\sigma_{ff}}{r} \right)^6 \right). \quad (9)$$

The external potential  $V_{ext}$ , which is included in the expression for the free energy Eq. (1), defines the interaction between the fluid molecules and the wall. In this paper we used the Still's 10-4-3 potential [15, 28], the expression for it can be found in the appendix A.

From the equality to zero of the  $\Omega$ -potential variation in equilibrium, taking into account Eq. (3)–(6), one can obtain an expression for the density

$$\hat{\rho}(\mathbf{r}) = \rho^{bulk} \exp \left\{ \frac{1}{k_B T} \left( -\frac{\delta F^{hs}[\rho(\mathbf{r})]}{\delta \rho(\mathbf{r})} - \frac{\delta F^{att}[\rho(\mathbf{r})]}{\delta \rho(\mathbf{r})} - V_{ext}(\mathbf{r}) + \mu^{HS} + \mu^{att} \right) \right\}, \quad (10)$$

where  $\mu^{att}$  and  $\mu^{hs}$  — chemical potentials, the expression of which can be found in the appendix A, the expression for the Helmholtz free energy variation are also given in the appendix A.

In Eq. (10) the density is implicitly included in the right-hand side through the Helmholtz energy variation. The Picard method is not the only method for solving nonlinear equation but it is the most popular and widely used for solving nonlinear equations, in particular for DFT equations [21, 27]. The bulk fluid density is chosen as the initial approximation (the stability and the rate of convergence of the method depend on the choice of the initial guess). At the next iteration step, the solution is defined as the sum of solutions at the previous and current iterations.

$$\rho^{j+1} = (1 - \gamma)\rho^j + \gamma\hat{\rho}^j \quad (11)$$

The parameter  $\gamma \in [0, 1]$  determines the degree of confidence in the new decision on the next iteration, the higher it is, the faster the algorithm converges, but at too high values of  $\gamma$ , the solution will be unstable and will not converge. Picard iteration method is highly reliable, so it often works for a long time. Also, for this method to work, it is necessary to calculate the Helmholtz free energy variation, and it imposes some restrictions on the form of the Helmholtz energy. The complication of the model, such as taking into account the surface heterogeneity [11–13] or the Coulomb interaction [1], leads to a change in the Helmholtz free energy form, which entails a change in the corresponding variations. It becomes necessary to change almost every term in Eq. (10) and add new ones. In work [11], it is clearly seen how taking into account the surface heterogeneity can strongly affect the expressions for variations, and what difficulties may arise in calculating the equilibrium density, even though the considered fluid is simple to model.

### III. VARIATION FREE METHOD

Variation Free Density Functional Theory uses stochastic optimization methods instead of classical DFT, which uses the Picard iteration method to find the equilibrium fluid density. The use of stochastic optimization methods, such as the genetic algorithm (GA) and particle swarm optimization (PSO), makes it possible to find the equilibrium density  $\rho^*(z)$  without calculating variations and to reduce the search time for a solution. The lack of need to take into account the variation of free energy is the main advantage of the VF-DFT. The form of the Helmholtz free energy is different for systems, consequently, its variation is also different. For some systems calculating the variation is a very laborious task due to the complex structure of the system's free energy. For example, for studying graphene nanobubbles by classical density functional and elasticity theories [20] it is important to know the energy of whole system and density distribution at the same time, because this system have an additional constraints for fluids molecule. Another example, in work [11], from the standard model of gas adsorption on an ideally smooth surface, they passed to the consideration of adsorption on a heterogeneous surface; this entailed significant changes in the variation of the Helmholtz energy. Also, the behavior of complex fluid with different types of interactions are interesting in some cases. For this purpose, the Statistical Associating Fluid Theory (SAFT) [22, 31, 32] is actively developed; due to the consideration of chain types of bonds in the molecule, association, dispersion contribution, an additional term appears in the free energy expression. All the of types the interaction might be expressed in a different way in Helmholtz free energy, for which it is also necessary to calculate the variation. In addition to the fact that it is necessary to choose a physical model and the corresponding type of free energy, the problems under study

are often endowed with specific geometric properties, and these properties dictate the coordinate system for DFT model [21]. The calculation of variations is simplified, but one coordinate system's transition can cause difficulties from the recalculating variations. For some physical systems it is not always possible to calculate the density variation without resorting to any tweaks and simplifications of the model (especially systems with additional constraints), because of the Helmholtz energy's complex structure. The use of the VF-DFT will detour these barriers and get enough accurate solutions, knowing only the Helmholtz free energy.

### A. Basic patterns analysis

The task of the system free energy optimization has a large search space. The information about the desired function's characteristic behavior could be used to reduce the search space dimension, isolate the basic patterns, and seek the fluid density as a linear combination of functions that contain that information. In such a representation of the sought function, the problem of finding the equilibrium density is reduced to finding the optimal expansion coefficients of  $a_i$  that would minimize the  $\Omega$ -potential  $\Omega[\rho(z)] = \Omega[a_i]$ . The quality and speed of search solutions will affect the number and type of basis functions.

A dataset  $\mathbf{X}$  of functions nitrogen density at 77.4 K and different relative pressures (from  $10^{-6}$  to 0.99) was created. So basis functions most accurately describe the behavior of the density of any fluid in the pore. These density functions were computed by the classical DFT once for all considered cases in section IV. Also, in order to add as much information as possible about the behavior of the desired function to the basis, the equilibrium densities of fluids with molecular radii from 0.85 Å, to 2 Å at a temperature of 77.4 K were taken, the other interaction parameters correspond to the parameters of nitrogen and have been fixed. Such a selection of basis functions does not limit the range of applicability of the algorithm. In section IV, it will be demonstrated that the VF-DFT is applicable for fluid other than nitrogen with other thermodynamic conditions. As a result, we got a dataset  $\mathbf{X}$  of 140 vectors Fig. 2a.

It is necessary to apply the Principle Component Analysis (PCA) [33] to  $\mathbf{X}$  with a variety of solutions, to identify the characteristic patterns for the function of density and most accurately describe the behavior of an arbitrary density of the fluid in the pore.

Let the column vector  $\mathbf{x}$  be one of the density distributions (there are 140 of them in our work). We normalize the matrix  $\mathbf{X}(N_x \times N_s)$ ,  $N_x = 2401$  — dimension in  $\rho$ ,  $N_s = 140$  — number of samples, as follows:

$$\mathbf{X}(:, i) = \mathbf{x} - \mathbf{x}_{mean}, \quad (12)$$

where  $\mathbf{x}_{mean}(N_x \times 1)$  is the average density distribution

over the dataset  $\mathbf{X}$ .

According to [34], we decompose the centered  $\mathbf{X}$  matrix using the Singular Value Decomposition (SVD):

$$\mathbf{X} = \mathbf{U} \cdot \mathbf{\Sigma} \cdot \mathbf{V}^T, \quad (13)$$

where  $\mathbf{U}(N_x \times N_s)$  — the matrix of left singular vectors (orthonormal basis),  $\mathbf{\Sigma}(N_s \times N_s)$  — a square diagonal matrix containing singular numbers, sorted in descending order,  $\mathbf{V}(N_s \times N_s)$  — a matrix of right singular vectors (also an orthonormal basis). As shown below, the left singular vectors carries information about unknown patterns, and their corresponding singular values indicate how common this pattern in the dataset. To facilitate the calculation in the PCA were applied truncated SVD, by selecting the number of components  $K$  by the energy criterion to  $\mathbf{\Sigma}$ . The square of the singular number is equal the variance in the corresponding direction in the feature space. The projection on this direction will be minimal. The basis element energy is a square of the singular number, normalized to the sum of squares singular numbers. Respectively, the more energy, the better the selected components will describe the original dataset [23].

$$I = \sigma^2 / \sum \sigma^2. \quad (14)$$

Thus,  $\mathbf{X} \approx \widetilde{\mathbf{X}} = \widetilde{\mathbf{U}} \cdot \widetilde{\mathbf{\Sigma}} \cdot \widetilde{\mathbf{V}}^T$ . For the dataset  $\widetilde{\mathbf{X}}$  can be calculated the sample (estimated) covariance matrix  $\mathbf{Q} = \widetilde{\mathbf{X}} \cdot \widetilde{\mathbf{X}}^T / (N_s - 1)$ . Note that,  $\widetilde{\mathbf{X}} \cdot \widetilde{\mathbf{X}}^T = \widetilde{\mathbf{U}} \cdot \widetilde{\mathbf{\Sigma}} \cdot \widetilde{\mathbf{V}}^T \cdot \widetilde{\mathbf{V}} \cdot \widetilde{\mathbf{\Sigma}}^T \cdot \widetilde{\mathbf{U}}^T = \widetilde{\mathbf{U}} \cdot \widetilde{\mathbf{\Sigma}}^2 \cdot \widetilde{\mathbf{U}}^T$ , i.e. squared singular values of  $\widetilde{\mathbf{X}}$  equal eigenvalues  $\mathbf{S}$  matrix  $\mathbf{Q}$  multiplied at  $1/(N_s - 1)$ , and the left singular vectors  $\widetilde{\mathbf{U}}$  are equal to the eigenvectors of the covariance matrix  $\mathbf{Q}$ . Knowing  $\widetilde{\mathbf{U}}$  and  $\mathbf{S}$ , the approach from [35] could be used, in which a new implementation is generated using a sample covariance matrix as follows:

$$\mathbf{x}_{new} = \widetilde{\mathbf{U}} \cdot \mathbf{S} \cdot \mathbf{a} + \mathbf{x}_{mean}. \quad (15)$$

Here  $\mathbf{a}$ — vector  $K \times 1$  from the Gaussian distribution  $\mathcal{N}(0, 1)$ , it can be interpreted as a vector of optimized parameters (components of this vector in fact are the coefficients of expansion of the desired density of the basis functions, which contain information about the characteristic behavior of the density of the fluid near the walls). During the optimization, the coefficients of the vector  $\mathbf{a}$  will be changing and the vector  $\mathbf{x}_{new}$  will be changing for minimizing the  $\Omega$  potential.

As a result, after principal component analysis (PCA) based on the  $\mathbf{X}$  matrix, a new basis of 10 vectors was calculated (the view of the first five principal components of the basis on Fig. 2b), which cover 95% of information by energy criterion. This means that instead of searching for 140 unknown numbers  $\mathbf{a}$ , we have to search for only 10, and the quality of this approach will practically not differ from the solution with the search for all 140 coefficients.

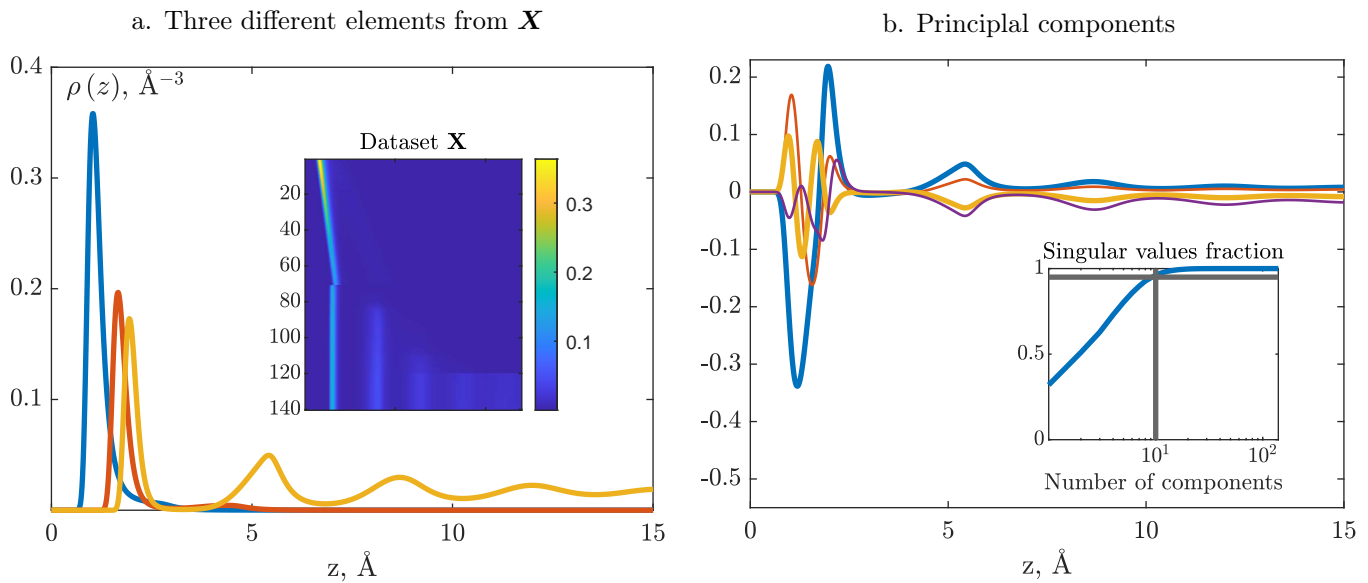


Figure 2: a) Three different elements  $\rho(z)$  from dataset  $\mathbf{X}$ ; dataset  $\mathbf{X}$  which contains 140 different fluid density distributions. b) Four principle components from  $\mathbf{X}$ . The relative error of reconstruction  $\mathbf{X} \sim 4\%$

## B. Stochastic optimization

As we have seen, the optimization problem is characterized by the fact that calculating the free energy variation is quite analytically tricky and change of the Helmholtz potential leads to recalculation of each term in Eq. (10). In this work, stochastic optimization was applied, the investigated function is used as a black box, without calculating variations. The required function is represented as Eq. (15), and optimization algorithms select the elements of the vector  $\mathbf{a}$  to minimize the free energy functional  $\Omega[\mathbf{a}]$ . The dimension of the optimization problem is equal to the dimension of the vector  $\mathbf{a}$ . In our cases this dimension is equal to  $10 \times 1$ . We considered two iterative heuristic approaches— GA and PSO, which are widely used in science and technology and have proven themselves in many industries [36–39]. This section will present a brief description of the algorithms principles and recommendations about how to configure their settings.

### 1. Genetic Algorithm (GA)

Darwin’s theory of evolution inspired the creation of a genetic algorithm. The algorithm is based on the idea that the fittest individuals, which evolve, inherit traits from their parents, mutate, and it is they who survive ("the fittest survives"). GA has been successfully applied to solve a wide variety of problems from various disciplines: feature selection in machine learning, image processing [40–42]. It is not possible to describe all the modifications and methods developed on the basis of the classical genetic algorithm. The most complete presen-

tation can be found in the articles [36, 39].

*Initialization:* we will call the vector  $\mathbf{a}$  a chromosome, a set of chromosomes— a generation. We recommend taking  $N_c$  chromosomes equal to the number of parameters to be optimized, in our case,  $N_c = 10$ . First, all the chromosomes are set randomly within the given boundaries. So  $\mathbf{a}$  is the vector of random variables from the  $\mathcal{N}(0, 1)$  on  $[0; 1]$ , and the boundaries might be taken as  $\pm 4\sigma$ . The objective function (fitness function) is calculated — in the minimization problem, the smaller it is, the more the chromosome is "adapted". In our case, the role of the objective function is played by the Omega potential  $\Omega[\mathbf{a}]$ . In the genetic algorithm, each iteration is the process of forming a new generation from a current generation. This process takes place with the help of genetic operators. We used the most basic operators and will describe them in more detail.

*Elitism:* one chromosome with the best objective function value is transferred to the new generation from the current generation without changes. This allows us at least not to lose the best solution, which ensures the loosely monotonous convergence of the algorithm.

*Crossover:* each new chromosome ( $N_c - 1$ ) is obtained by crossing a pair of parents. The probability of selecting a current chromosome crossing generation can be either predetermined or depend on the fitness function (roulette wheel [36]). The use of one or another approach changes the algorithm’s exploration and exploitation properties; in this work, a combined approach is used. In this work, the index crossing approach was used. Several points in the current chromosomes are selected, and all genes with indices between the chosen points are exchanging occurs in blocks of genes.

*Mutation:* a new chromosome obtained at the previous

stage of crossing from a pair of parental ones undergoes mutation with a given probability, i.e. random changing one or more of its components. A high mutation rate slows down the convergence of the algorithm but makes it possible to find the global optimum more successfully. The level of mutation in this work was determined at the level of 0.5 — this means that half of the population's chromosomes are subject to mutation.

After the new generation's formation for all chromosomes, the fitness function is calculated (if it was not known). The algorithm stops when the allotted number of fitness calls is reached.

## 2. Particle Swarm Optimization (PSO)

Genetic algorithms today are one of the most popular tools for solving optimization problems. However, their use is not without its drawbacks. The solution converges to the optimum only after a large number of calculations, while it is not guaranteed that the minimum will be global. There is no clear criterion for stopping in case of insufficient mutation, the solution can be in a local minimum for a very long time, monotonic convergence is not guaranteed. All this leads to the emergence of new, more developed GA, the use of GA in conjunction with other algorithms, as well as the development of new stochastic approaches.

Particle Swarm Optimization is one such approach which was constructed on the base of GA. It was first developed in 1995 by Kennedy, Eberhart and Shi [43] to study the behavior of a swarm of insects or schools of fish that move around space in search of food. Later it was simplified and applied to solve various optimization problems [44]. Let us consider this method in more detail, using the terminology from [37].

*Initialization:* the vector  $\mathbf{a}$  is called a particle, the set of particles is a swarm (by analogy with a chromosome and a generation). As in GA, each particle stores its current position  $\mathbf{x}_i^k$  and the corresponding objective function value  $F^{obj}(\mathbf{x})$ . In addition, as well as a velocity vector  $\mathbf{v}_i^k$  (the same size as the position vector). In addition, for each particle, the best value of the objective functional is stored, at any iteration achieved by it and the corresponding position. The objective function ( $\Omega$ -potential) is the smaller, the better.

The number of particles in the work is set equal to the number of optimized coefficients (in our work it is ten), and the initial velocity is zero. The initial position of the particles is set from a uniform distribution.

PSO is an iterative algorithm in which the new position of particle  $i$  at iteration  $k + 1$ ,  $\mathbf{x}_i^{k+1}$ , is determined by adding speed term  $\mathbf{v}_i^{k+1}$  to  $\mathbf{x}_i^k$ :  $\mathbf{x}_i^{k+1} = \mathbf{x}_i^k + \mathbf{v}_i^{k+1}$ . The  $\mathbf{v}_i^{k+1}$  components are calculated as follows:

$$\mathbf{v}_i^{k+1} = \omega \mathbf{v}_i^k + c_1 \mathbf{r}_1 (\hat{\mathbf{y}}_i^k - \mathbf{x}_i^k) + c_2 \mathbf{r}_2 (\tilde{\mathbf{y}}^k - \mathbf{x}_i^k), \quad (16)$$

where  $\omega$ ,  $c_1$ ,  $c_2$  are some weights indicating the degree of attractiveness of a particular direction,  $\mathbf{r}$  is the random variables in the range from 0 to 1.

It can be seen from the Eq. (16) that the speed is made up of three components, called inertial, cognitive and social, respectively. The inertial component  $\omega \mathbf{v}_i^k$  is responsible for the movement of the particle in the direction in which it moved at the previous iteration  $k$ . The cognitive term  $c_1 \mathbf{r}_1 (\hat{\mathbf{y}}_i^k - \mathbf{x}_i^k)$  is responsible for movement depending on the previous best position for the particle  $i$ . The social component  $c_2 \mathbf{r}_2 (\tilde{\mathbf{y}}^k - \mathbf{x}_i^k)$  includes information about the best position for all particles and is responsible for moving towards it. At each iteration, each particle in the swarm is moved to a new location in the search space, and for each location an objective function is calculated that determines how good the given solution is.

The algorithm stops when it reaches the allocated number of calls of the objective function, and the best position of the particle is considered for all iterations response.

In this work, the coefficients  $\omega = 0.7298$ ,  $c_1 = 1.4962$ ,  $c_2 = 1.4962$ . These values are the most versatile and suitable for many applications, it is worth noting that these three factors can not be arbitrary, and are related in [45]. Changing these parameters did not give a better value of the objective function and did not reduce the time of calculation for our cases.

## C. Hybrid Density Functional Theory (H-DFT)

The VF-DFT approach does not require the calculation of the Helmholtz energy variation and allows a faster solution than the classical DFT with Picard iteration. However, classic DFT provides a more accurate solution. To maintain the advantages in computation's speed up and quality of the solution from both approaches, it was decided to combine them into a single algorithm called Hybrid Hybrid Density Functional Theory (H-DFT) Fig. 3. At the initial stage of H-DFT, the approximate solution is sought via VF-DFT and stochastic optimization techniques. Then, the solution which produces VF-DFT is supplied as an initial approximation to the classical DFT Picard iteration. This combination made it possible to obtain a significant gain in the speed of density calculation, in comparison with the classical DFT (the results on speed and quality are given in the section IV), while the quality of the solution remained at the same level as that of the classical algorithm. Due to the fact that the VF-DFT solution is close to equilibrium, for Picard iteration, the value of  $\gamma$  could be set large enough. This affects the speed of Picard iteration and the number of iterations required for the algorithm.

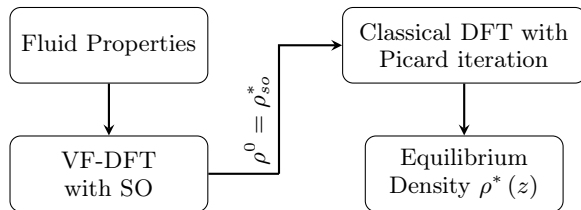


Figure 3: Scheme of Hybrid Density Functional Theory

#### IV. RESULTS

This section presents the results for VF-DFT and H-DFT methods. GA and PSO are used for seeking optimal coefficients of expansion for desired fluid density in the pore. The developed methods were compared with the classical DFT in terms of calculation time and the value of  $\Omega$ -potential. Methods are tested for nitrogen and argon in the pore of 3.6 nm. Fluid-fluid and solid-fluid are shown in the table I. The parameters for solid-fluid interaction were calculated according to the Lorentz-Berthelot rule Eq. (17), where  $\varepsilon_{ss} = 28$  K,  $\sigma_{ss} = 3.4$  Å

$$\varepsilon_{sf} = \sqrt{\varepsilon_{ss}\varepsilon_{ff}}, \quad \sigma_{sf} = \frac{1}{2}(\sigma_{ss} + \sigma_{ff}), \quad (17)$$

Table I: The fluid-fluid and solid-fluid interaction parameters. For LJ potential cut off distance was taken  $r_{cut} = 5\sigma_{ff}$ . Pore wall surface density  $\rho_V = 0.114$  Å<sup>-3</sup>, distance between layers of carbon atoms  $\Delta = 3.35$  Å

Fluid	$T$ , K	Fluid-Fluid		Solid-Fluid	
		$\varepsilon_{ff}/k_B$ , K	$\sigma_{ff}$ , Å	$\varepsilon_{sf}/k_B$ , K	$\sigma_{sf}$ , Å
$N_2$	77.4	94.45	3.575	51.43	3.487
$Ar$	87.3	111.95	3.358	55.99	3.379

##### A. Basis functions and problem statement for identical fluids

Nitrogen was taken in the first step of testing the algorithm because the dataset contains the most information about this fluid. As already mentioned, the basis was constructed from the dataset of equilibrium nitrogen densities  $\mathbf{X}$  in the pore of 3.6 nm at a fixed temperature of 77.4 K and different relative pressures. The basis also includes the equilibrium densities of “artificial” fluids with different molecular radii (from 0.85 Å to 2 Å) with the rest of the interaction parameters fixed. All problems below use the same basis.

*a. High pressure.* When calculating the equilibrium density at large values of relative pressure, as a fact, classical algorithms are looking for an equilibrium solution

for a long time. It is in such problems that the variation free approach gives the most significant gain in computation time. Even though Picard iteration is very reliable, to ensure convergence in such problems, the  $\gamma$  parameter is chosen very small, dramatically affecting the convergence rate. The Fig. 4a shows the nitrogen density in a pore of 3.6 nm at a temperature of 77.4 K and a relative pressure in the bulk  $P/P_0 = 0.6924$  ( $P_0$  is the saturation pressure). It is important to note that the dataset does not include a function at the relative pressures at which calculations are made in the cases under consideration. The difference in calculation time is significant, and the solution is quite close in the value of the  $\Omega$  potential to the classical DFT.

The value of the  $\Omega$ -potential for the Picard iteration method decreases much more slowly compared to the VF-DFT, as seen in Fig. 5.

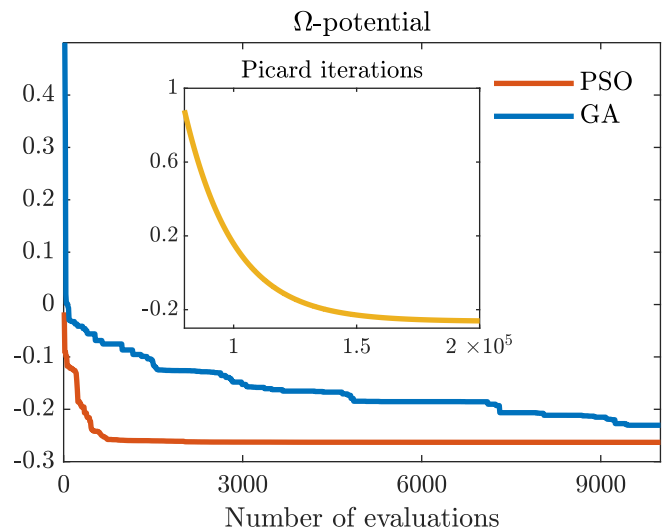


Figure 5: The value of  $\Omega$  potential with iterations for classical DFT (yellow solid line), and  $\Omega$  potential with evaluation for VF-DFT with PSO (red solid line) and GA (blue dashed line)

It can also be noted Fig. 5 that the behavior of the  $\Omega$  potential for stochastic algorithms is not strictly monotone. This is due to the principle of the algorithms themselves. There are no exact convergence criteria for stochastic algorithms, which means that the solution that the algorithm produces does not have to be acceptable. In this case, the calculation have to be continued with hope that the decision will be improved or run the algorithm again. Stability and speed of search procedure depends on settings of algorithm. Also, it should be noted the difference between iterations and evaluations. For example, if we have a population of  $N_c$  chromosomes, each of which gets evaluated once in a single iteration. This means that in every iteration of an algorithm, the evaluation function is called  $N_c$  times (once for each chromosome). Hence, we have the relationship:  $Number\ of\ evaluations = Number\ of\ iterations \cdot N_c$ .



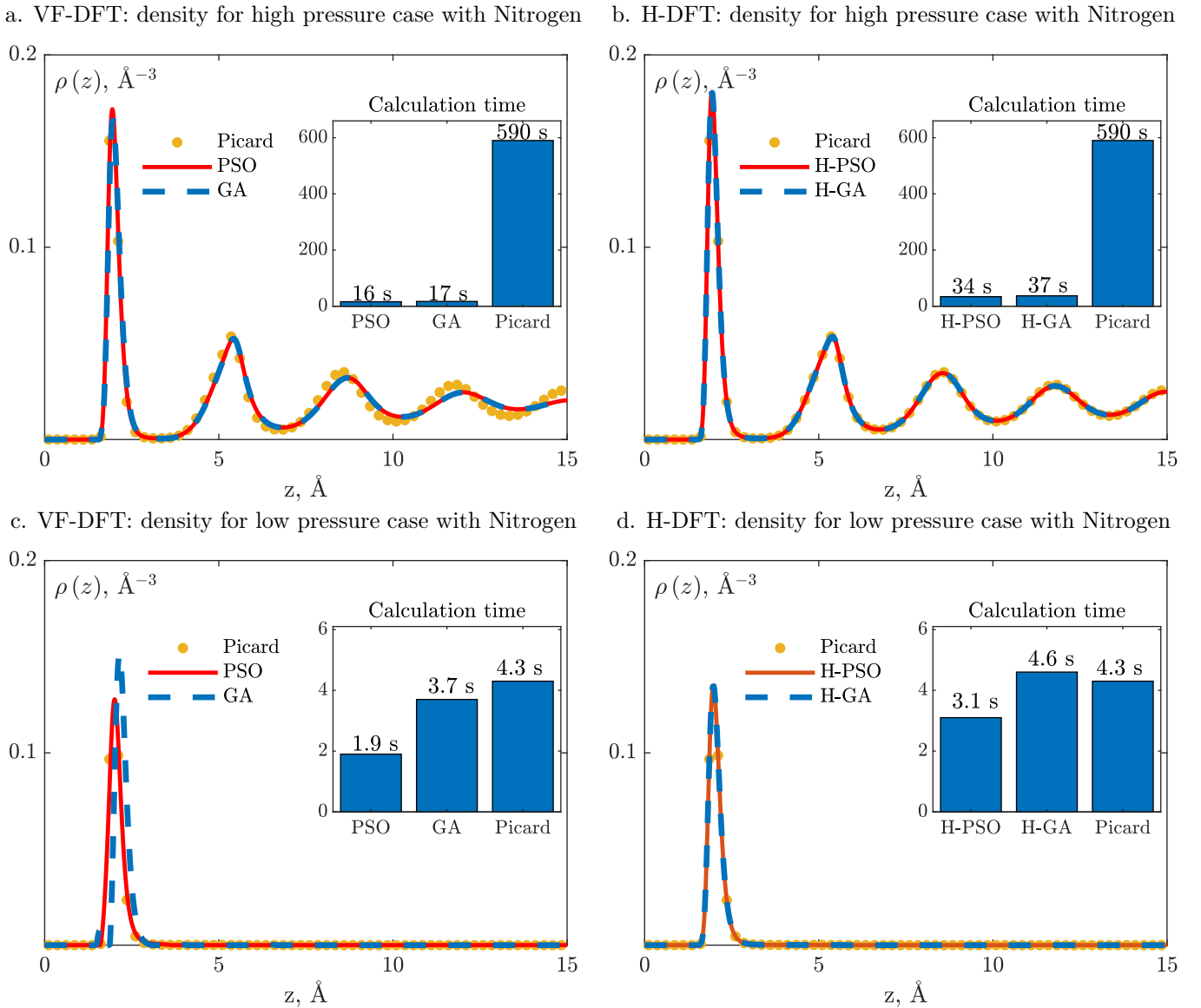


Figure 4: Red solid line – VF-DFT (H-DFT) with PSO, blue meshed line – VF-DFT (H-DFT) with GA, yellow circles indicate classic DFT with Picard iteration. a) VF-DFT equilibrium densities at  $P/P_0 = 0.6924$  for nitrogen  $\Omega_{PSO} = -0.2630$ ,  $\Omega_{GA} = -0.2628$ ,  $\Omega_{Pic} = -0.2634$ . b) H-DFT equilibrium densities at  $P/P_0 = 0.6924$  for nitrogen. The figures completely coincide, but the running time of hybrid methods is an order of magnitude less  $\Omega_{H-PSO} = \Omega_{H-GA} = \Omega_{Pic} = -0.2634$ . c) VF-DFT equilibrium densities at  $P/P_0 = 0.0044$  for nitrogen  $\Omega_{PSO} = -0.0305$ ,  $\Omega_{GA} = -0.0286$ ,  $\Omega_{Pic} = -0.0308$ . d) H-DFT equilibrium densities at  $P/P_0 = 0.0044$  for nitrogen  $\Omega_{H-PSO} = \Omega_{H-GA} = \Omega_{Pic} = -0.0308$

VF-DFT algorithms with GA, PSO managed with the task an order of magnitude faster, but the quality of the solutions obtained is slightly inferior to the classical DFT based on Picard iteration. However, it should be noted that the structural feature of the VF-DFT fluid behavior was reproduced well, the number of peaks and their shapes are in good agreement with the solution of the classical approach. PSO-based VF-DFT provided the value of the  $\Omega$  potential for the calculated equilibrium density  $\Omega[\rho_{PSO}^*] = -0.2630$ , GA-based VF-DFT

$\Omega[\rho_{GA}^*] = -0.2628$ , both turned out to be very close to the value given by the DFT with the Picard iteration method  $\Omega[\rho_{Pic}^*] = -0.2634$ .

The Fig. 4b shows the result of hybrid methods versus Picard iteration. The running time is slightly different from the VF-DFT, but the final value of the  $\Omega$  potential for all three density profiles is the same  $\Omega[\rho_{H-PSO}^*] = \Omega[\rho_{H-GA}^*] = \Omega[\rho_{Picard}^*] = -0.2634$ .

Variation free approach makes it possible to obtain a decision in a few times faster, and the association of VF-

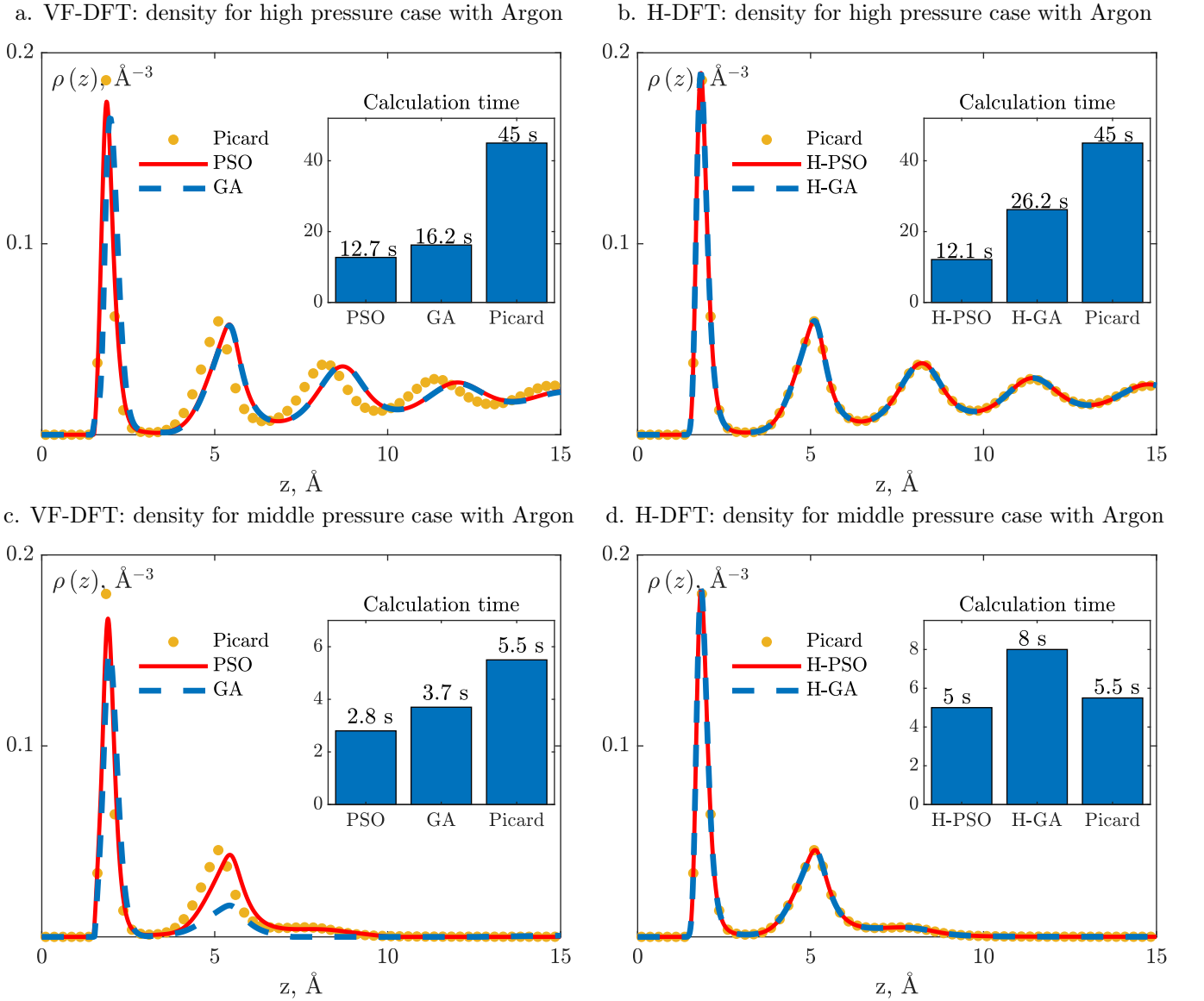


Figure 6: Red solid line – VF-DFT (H-DFT) with PSO, blue meshed line – VF-DFT (H-DFT) with GA, yellow circles indicate classic DFT with Picard iteration a) VF-DFT equilibrium densities at  $P/P_0 = 0.9932$  for argon  $\Omega_{PSO} = -0.1674$ ,  $\Omega_{GA} = -0.1626$ ,  $\Omega_{Pic} = -0.1712$  b) H-DFT equilibrium densities at  $P/P_0 = 0.9932$  for argon  $\Omega_{H-PSO} = \Omega_{H-GA} = \Omega_{Pic} = -0.1077$ . c) VF-DFT equilibrium densities at  $P/P_0 = 0.4739$  for argon  $\Omega_{PSO} = -0.1049$ ,  $\Omega_{GA} = -0.1019$ ,  $\Omega_{Pic} = -0.1077$  d) H-DFT equilibrium densities at  $P/P_0 = 0.4739$  for argon  $\Omega_{H-PSO} = \Omega_{H-GA} = \Omega_{Pic} = -0.1077$

DFT with classical DFT provides, in addition to high-speed computing, great quality solutions.

*b. Low pressure.* The Fig. 4c shows that at low relative pressures  $P/P_0 = 0.0044$ , the computation speed for VF-DFT is not as significant as at high pressures. At low relative pressures, classical algorithms work faster than at high pressures, due to the choice of the parameter  $\gamma$  large enough.

For hybrid algorithms Fig. 4d, it turned out that the genetic algorithm is slower than Picard iteration, VF-DFT with PSO is still faster than both, and the value of

the  $\Omega$  potential for all three is the same  $\Omega[\rho_{H-PSO}^*] = \Omega[\rho_{H-GA}^*] = \Omega[\rho_{Pic}^*] = -0.0308$ .

In this case, the speed of the algorithms is significantly affected by the initialization time of the optimization algorithms, and for hybrid algorithms this time is longer, since, in addition to stochastic PSO and GA, it is required to initialize Picard iteration for which the variation must also be calculated.

## B. Basis functions and problem statement for different fluids

This section represents the most valuable results from the VF-DFT Fig. 6. To make sure that VF-DFT can be used not only for calculating the equilibrium nitrogen density at a temperature of 77.4 K (the basis was considered based on nitrogen), but also for other fluids, it was decided to apply VF-DFT for argon at a temperature of 87.3 K. The results of this section confirm the idea of VF-DFT applicability for calculating the density of a fluid with a complex structure of Helmholtz free energy without calculating variations.

*a. High pressure.* The Fig. 6a shows that the peaks position did not coincide exactly, but it is worth noting that the number and size of the peaks VF-DFT was able to restore. Also, VF-DFT still handles calculations many times faster than the classic DFT with Picard iteration.

When using the hybrid algorithm Fig. 6b, the solutions completely coincided with a shorter calculation time.

*b. Middle pressure.* As the relative pressure decreases, the VF-DFT provide a smaller gain in speed Fig. 6c. In this case, the algorithms were able to catch the peaks' position, but only VF-DFT with PSO was able to recover the magnitude of the peaks.

The hybrid approach in the case with relative pressure  $P/P_0 = 0.4739$  Fig. 6d did not give the expected gain in the calculation speed. The GA-based H-DFT turned out to be even slower than the classical DFT. As already noted in the section with the nitrogen results, this is due to the initialization time optimization algorithms. At such pressures, in the Picard iteration for argon, a sufficiently large value of  $\gamma$  can be used. The time spent in the H-DFT to obtain an approximate solution turned out to be very close to the time DFT with Picard iterations.

In all considered cases, the greatest gain in speed was obtained at high relative pressures. This is due to the fact that at high relative pressures, for the convergence of the Picard iteration method, it is necessary to choose a sufficiently small parameter  $\gamma$ . But in addition, at high relative pressures, more layers are formed near the wall, which means more patterns that can be distinguished using PCA. Thus, it turns out that it is easier to build a solution using VF-DFT at high pressures.

## V. CONCLUSION

Density functional theory is a powerful tool for investigating the behavior of fluids and surfaces, taking into account molecular forces at the nanoscale. The Variation Free DFT approach developed in this work for finding the equilibrium density is of interest for the study of intricate systems: systems with additional constrains, complex fluids. Besides, the combination of VF-DFT, which uses stochastic optimization methods, with the classical DFT with Picard iteration made it possible to significantly speed up the calculation for high relative pressure

cases while maintaining the solution quality as in the classical DFT. At low relative pressures, the calculation speed gain is not as significant as at high pressures because of specific pattern extraction from dataset for the high relative pressure. The combined algorithm can be applied to speed up calculations of the equilibrium fluid density at high pressures, in particular, to speed up the calculation of the adsorption isotherm or pore stresses. It should be noted that the VF-DFT solution's speed and quality directly depend on the type of basis functions. The size of the basis and the type of basis functions can be changed, improved, and refined to obtain a better solution with a minimum cost of calculation time. In addition to the basis, the speed of VF-DFT operation is influenced by setting the optimization algorithms' parameters. The optimization algorithms GA and PSO considered in this work showed promising results, but PSO has a higher quality and speed of finding a solution. In the future, it is possible to investigate the variation free approach with other optimization methods, investigate systems for which the Helmholtz free energy has a complex form or systems with specific constraints.

## ACKNOWLEDGMENTS

The authors are grateful to Timur Aslyamov for critical comments and fruitful discussions about this work.

## Appendix A: Details for Density Functional Theory

The Eq. (7) on the page 3 contains weighted density functions  $n_\alpha$ , which are defined as follows:

$$n_\alpha(\mathbf{r}) = \int d^3r' \rho(\mathbf{r}') \omega_\alpha(\mathbf{r} - \mathbf{r}'), \quad (\text{A1})$$

where  $\omega_\alpha$  — weight functions;  $\omega_3(\mathbf{r}) = \theta(R - r)$ ,  $\omega_2(\mathbf{r}) = \delta(R - r)$ ,  $\omega_1(\mathbf{r}) = \frac{r}{R} \delta(R - r)$ ,  $\omega_0 = \frac{\omega_2}{4\pi R^2}$ ,  $\omega_1 = \frac{\omega_2}{4\pi R}$ ,  $\delta$  и  $\theta$  — Dirac delta function and Heaviside theta function,  $R$  — fluid particle radius.

Similarly, the Helmholtz energy Eq. (3), the chemical potential of the fluid can also be divided into the sum of three components

$$\mu(\rho) = \mu_{id}(\rho) + \mu_{HS}(\rho) + \mu_{att}(\rho) \quad (\text{A2})$$

$$\mu_{id}(\rho) = k_B T (\ln \lambda^3 \rho^{bulk}) = const \quad (\text{A3})$$

$$\mu_{HS}(\rho) = k_B T \left( \sum \frac{\partial \Phi}{\partial n_\alpha} \frac{\partial n_\alpha}{\partial \rho} \right) = const \quad (\text{A4})$$

$$\mu_{att}(\rho) = \rho^{bulk} \int d^3r U_{att}(r) = const \quad (\text{A5})$$

where  $\rho^{bulk}$  — fluid density in the bulk.

In this paper, the pores of the slit geometry are considered. The problem is symmetric in two directions ( $x$ ,  $y$ ), and the density depends only on one coordinate

$z$ :  $\rho(\mathbf{r}) = \rho(z)$ . The pore walls are composed of carbon atoms. The potential of fluid-solid interaction is described by the Still potential 10-4-3 [28].

$$V_{sf}(z) = 2\pi\varepsilon_{sf}\rho_V\sigma_{sf}^3\Delta\left(\frac{2}{5}\left(\frac{\sigma_{sf}}{z}\right)^{10} - \left(\frac{\sigma_{sf}}{z}\right)^4 - \frac{\sigma_{sf}^4}{3\Delta(0.61\Delta+z)^3}\right). \quad (\text{A6})$$

Full potential in the pore from two walls:

$$V_{ext}(z) = V_{sf}(z) + V_{sf}(H_{cc} - z), \quad (\text{A7})$$

$\rho_V$  – the density of the wall material,  $\Delta$  – the distance between the layers of wall atoms,  $H_{cc}$  – pore diameter calculated between the centers of the carbon atoms of opposing sides, the width of the pores accessible to fluid  $H = H_{cc} - 2z_0 + \sigma_{ff}$ , where  $z_0$  – penetration rate ( $z_0 = 0.9\sigma_{sf}$ ).

In the case of a planar geometry could be write down analytic form Helmholtz free energy variation, for hard sphere repulsion:

$$\frac{\delta F^{HS}[\rho]}{\delta\rho(z)} = \sum_{\alpha} \int dz' \frac{\partial\Phi[n_{\alpha}]}{\partial n_{\alpha}} \frac{\delta n_{\alpha}(z')}{\delta\rho(z)} \quad (\text{A8})$$

where, taking into account the type of potential attraction interaction  $U_{att}(r)$  при  $|\Delta z| \leq \lambda$

$$G(z_1, z_2) = 2\pi \left\{ \int_0^{\sqrt{\lambda^2 - \Delta z^2}} -\varepsilon_{ff} r dr + \int_{\sqrt{\lambda^2 - \Delta z^2}}^{\sqrt{r_{cut}^2 - \Delta z^2}} dr 4\varepsilon_{ff} r \left[ \frac{\sigma_{ff}^{12}}{(\Delta z^2 + r^2)^6} - \frac{\sigma_{ff}^6}{(\Delta z^2 + r^2)^3} \right] \right\} =$$

$$= -\pi\varepsilon_{ff}(\lambda^2 - \Delta z^2) + \frac{4}{5}\pi\varepsilon_{ff}\sigma_{ff}^{12} \left( \frac{1}{\lambda^{10}} - \frac{1}{r_{cut}^{10}} \right) - 2\pi\varepsilon_{ff}\sigma_{ff}^6 \left( \frac{1}{\lambda^4} - \frac{1}{r_{cut}^4} \right), \quad (\text{A11})$$

where  $|\Delta z| > \lambda$  and  $|\Delta z| \leq r_{cut}$

$$G(z_1, z_2) = 2\pi \int_0^{\sqrt{r_{cut}^2 - \Delta z^2}} dr 4\varepsilon_{ff} r \left[ \frac{\sigma_{ff}^{12}}{(\Delta z^2 + r^2)^6} - \frac{\sigma_{ff}^6}{(\Delta z^2 + r^2)^3} \right] =$$

$$= \frac{4}{5}\pi\varepsilon_{ff}\sigma_{ff}^{12} \left( \frac{1}{\Delta z^{10}} - \frac{1}{r_{cut}^{10}} \right) - 2\pi\varepsilon_{ff}\sigma_{ff}^6 \left( \frac{1}{\Delta z^4} - \frac{1}{r_{cut}^4} \right), \quad (\text{A12})$$

with  $|\Delta z| > r_{cut}$ ,  $G(z_1, z_2) = 0$ .

Thus, the variation of the Helmholtz energy from attrac-

tion interaction

$$\frac{\delta F^{att}[\rho(z)]}{\delta\rho(z)} = \frac{k_B T}{2} \int dz' \rho(z') G(z - z') \quad (\text{A13})$$

- [2] S. Rezaei Gomari, Y. Gorra Diallo Omar, F. Amrouche, M. Islam, and D. Xu, New insights into application of nanoparticles for water-based enhanced oil recovery in carbonate reservoirs, *Colloids and Surfaces A: Physicochemical and Engineering Aspects* **568**, 164 (2019).
- [3] X. Wang, Z. Zhang, O. Torsæter, and J. He, Atomistic insights into the nanofluid transport through an ultra-confined capillary, *Physical Chemistry Chemical Physics* **20**, 4831 (2018).
- [4] A. V. Neimark, P. I. Ravikovitch, M. Grün, F. Schüth, and K. K. Unger, Pore size analysis of MCM-41 type adsorbents by means of nitrogen and argon adsorption, *Journal of Colloid and Interface Science* **207**, 159 (1998).
- [5] Y. X. Yu, J. Wu, and G. H. Gao, Density-functional theory of spherical electric double layers and  $\zeta$  potentials of colloidal particles in restricted-primitive-model electrolyte solutions, *Journal of Chemical Physics* **120**, 7223 (2004).
- [6] M. Müller and L. G. MacDowell, Wetting of polymer liquids: Monte carlo simulations and self-consistent field calculations, *Journal of Physics: Condensed Matter* **15**, R609 (2003).
- [7] I. Napari, A. Laaksonen, V. Talanquer, and D. W. Oxtoby, A density functional study of liquid-liquid interfaces in partially miscible systems, *The Journal of chemical physics* **110**, 5906 (1999).
- [8] K. Sumida, D. L. Rogow, J. A. Mason, T. M. McDonald, E. D. Bloch, Z. R. Herm, T. H. Bae, and J. R. Long, Carbon dioxide capture in metal-organic frameworks, *Chemical Reviews* **112**, 724 (2012).
- [9] P. I. Ravikovitch, A. Vishnyakov, and A. V. Neimark, Density functional theories and molecular simulations of adsorption and phase transitions in nanopores, *Physical Review E - Statistical Physics, Plasmas, Fluids, and Related Interdisciplinary Topics* **64**, 20 (2001).
- [10] G. O. Berim and E. Ruckenstein, Nanodrop on a nanorough solid surface: Density functional theory considerations, *Journal of Chemical Physics* **129**, 10.1063/1.2951453 (2008).
- [11] T. Aslyamov and A. Khlyupin, Density functional theory formulation for fluid adsorption on correlated random surfaces, *Journal of Chemical Physics* **147**, 1 (2017).
- [12] A. V. Neimark, Y. Lin, P. I. Ravikovitch, and M. Thommes, Quenched solid density functional theory and pore size analysis of micro-mesoporous carbons, *Carbon* **47**, 1617 (2009).
- [13] J. Jagiello and J. P. Olivier, 2D-NLDFT adsorption models for carbon slit-shaped pores with surface energetical heterogeneity and geometrical corrugation, *Carbon* **55**, 70 (2013).
- [14] K. Yang, Y. Lin, X. Lu, and A. V. Neimark, Solvation forces between molecularly rough surfaces, *Journal of Colloid and Interface Science* **362**, 382 (2011).
- [15] P. I. Ravikovitch, A. Vishnyakov, R. Russo, and A. V. Neimark, Unified approach to pore size characterization of microporous carbonaceous materials from N<sub>2</sub>, Ar, and CO<sub>2</sub> adsorption isotherms, *Langmuir* **16**, 2311 (2000).
- [16] T. Aslyamov, V. Pletneva, and A. Khlyupin, Random surface statistical associating fluid theory: Adsorption of n-alkanes on rough surface, *The Journal of chemical physics* **150**, 054703 (2019).
- [17] T. Aslyamov, A. Khlyupin, V. Pletneva, and I. Akhatov, Theoretical approach to rough surface characterization for silica materials, *The Journal of Physical Chemistry C* **123**, 28707 (2019).
- [18] P. B. Balbuena and K. E. Gubbins, Theoretical interpretation of adsorption behavior of simple fluids in slit pores, *Langmuir* **9**, 1801 (1993).
- [19] D. W. Oxtoby, Density Functional Methods in the Statistical Mechanics of Materials, *Annual Review of Materials Research* **32**, 39 (2002).
- [20] T. Aslyamov, E. Iakovlev, I. S. Akhatov, and P. Zhilyaev, Model of graphene nanobubble: Combining classical density functional and elasticity theories, *The Journal of Chemical Physics* **152**, 054705 (2020).
- [21] R. Roth, Fundamental measure theory for hard-sphere mixtures: A review (2010).
- [22] S. Xi, J. Liu, A. Valiya Parambathu, Y. Zhang, and W. G. Chapman, An efficient algorithm for molecular density functional theory in cylindrical geometry: Application to interfacial statistical associating fluid theory (isaft), *Industrial & Engineering Chemistry Research* **59**, 6716 (2020).
- [23] W. Sun and L. J. Durlofsky, A New Data-Space Inversion Procedure for Efficient Uncertainty Quantification in Subsurface Flow Problems, *Mathematical Geosciences* **49**, 679 (2017).
- [24] J. Wu, *Variational Methods in Molecular Modeling*, edited by J. Wu, Molecular Modeling and Simulation (Springer Singapore, Singapore, 2017) p. 324.
- [25] M. Edelmann and R. Roth, A numerical efficient way to minimize classical density functional theory, *Journal of Chemical Physics* **144**, 10.1063/1.4942020 (2016).
- [26] M. P. Sears and L. J. Frink, A new efficient method for density functional theory calculations of inhomogeneous fluids, *Journal of Computational Physics* **190**, 184 (2003).
- [27] J. Mairhofer and J. Gross, Numerical aspects of classical density functional theory for one-dimensional vapor-liquid interfaces, *Fluid Phase Equilibria* **444**, 1 (2017).
- [28] W. A. Steele, *The interaction of gases with solid surfaces*, Vol. 3 (Pergamon, 1974).
- [29] Y. Rosenfeld, Free-energy model for the inhomogeneous hard-sphere fluid mixture and density-functional theory of freezing, *Physical Review Letters* **63**, 980 (1989).
- [30] J. D. Weeks, D. Chandler, and H. C. Andersen, Role of repulsive forces in determining the equilibrium structure of simple liquids, *The Journal of Chemical Physics* **54**, 5237 (1971).
- [31] V. Papaioannou, F. Calado, T. Lafitte, S. Dufal, M. Sadegzadeh, G. Jackson, C. S. Adjiman, and A. Galindo, Application of the SAFT- $\gamma$  Mie group contribution equation of state to fluids of relevance to the oil and gas industry, *Fluid Phase Equilibria* **416**, 104 (2016).
- [32] T. Lafitte, A. Apostolou, C. Avendaño, A. Galindo, C. S. Adjiman, E. A. Müller, and G. Jackson, Accurate statistical associating fluid theory for chain molecules formed from Mie segments, *Journal of Chemical Physics* **139**, 10.1063/1.4819786 (2013).
- [33] M. Elizarev, A. Mukhin, and A. Khlyupin, Objective-sensitive principal component analysis for high-dimensional inverse problems, arXiv preprint arXiv:2006.04527 (2020).
- [34] H. Abdi and L. J. Williams, Principal component analysis. wiley interdisciplinary reviews: computational statistics, *Wiley Interdisciplinary Reviews: Computational Statistics* , 1 (2010).
- [35] P. Sarma, L. J. Durlofsky, K. Aziz, and W. H. Chen,

- Efficient real-time reservoir management using adjoint-based optimal control and model updating, *Computational Geosciences* **10**, 3 (2006).
- [36] A. Nejad Ebrahimi, S. Jamshidi, S. Iglauer, and R. Boozarjomehry, Genetic algorithm-based pore network extraction from micro-computed tomography images, *Chemical Engineering Science* **92**, 157 (2013).
- [37] J. E. Onwunalu and L. J. Durlafsky, Development and application of a new well pattern optimization algorithm for optimizing large-scale field development, *Proceedings - SPE Annual Technical Conference and Exhibition* **3**, 1926 (2009).
- [38] Eberhart and Yuhui Shi, Particle swarm optimization: developments, applications and resources, in *Proceedings of the 2001 Congress on Evolutionary Computation (IEEE Cat. No.01TH8546)*, Vol. 1 (IEEE, 2001) pp. 81–86.
- [39] G. Montes, P. Bartolome, and A. Udias, The Use of Genetic Algorithms in Well Placement optimization, in *Proceedings of SPE Latin American and Caribbean Petroleum Engineering Conference* (Society of Petroleum Engineers, 2001) pp. 1–10.
- [40] J. Huang, Y. Cai, and X. Xu, A hybrid genetic algorithm for feature selection wrapper based on mutual information, *Pattern Recognition Letters* **28**, 1825 (2007).
- [41] R. Ouellette, M. Browne, and K. Hirasawa, Genetic algorithm optimization of a convolutional neural network for autonomous crack detection, *Proceedings of the 2004 Congress on Evolutionary Computation, CEC2004* **1**, 516 (2004).
- [42] S. Sharma, H. Singh, and G. G. Balint-Kurti, Genetic algorithm optimization of laser pulses for molecular quantum state excitation, *Journal of Chemical Physics* **132**, 10.1063/1.3314223 (2010).
- [43] J. Kennedy and R. Eberhart, Particle swarm optimization, in *Proceedings of ICNN'95 - International Conference on Neural Networks* (IEEE, 1995).
- [44] A. Banks, J. Vincent, and C. Anyakoha, A review of particle swarm optimization. Part I: Background and development, *Natural Computing* **6**, 467 (2007).
- [45] I. C. Trelea, The particle swarm optimization algorithm: Convergence analysis and parameter selection, *Information Processing Letters* **85**, 317 (2003).